Evidence for Transmission of Ferromagnetic Interactions through Hydrogen Bonds in Alkyne-Substituted Nitroxide Radicals: Magnetostructural Correlations and Polarized Neutron Diffraction Studies

Francisco M. Romero,*,†,⊥ Raymond Ziessel,*,† Michel Bonnet,‡ Yves Pontillon,‡ Eric Ressouche,‡ Jacques Schweizer,*,‡ Bernard Delley,# André Grand,§ and Carley Paulsen||

Contribution from the Laboratoire de Chimie, d'Electronique et de Photonique Moléculaires, associé au CNRS ESA-7008, Ecole Chimie, Polymères, Matériaux (ECPM), 25 rue Becquerel -BP 08- 67087 Strasbourg Cedex, France, Département de Recherche Fondamentale sur la Matière Condensée, DRFMC/SPSMS/MDN and DRFMC/SCIB, CEA-Grenoble, 17 rue des Martyrs 38054 Grenoble Cedex, France, Paul Scherer Institute Zürich, Badenerstrasse 569, 8048 Zürich, Switzerland, and Centre de Recherche sur les Très Basses Températures, CNRS, rue des Martyrs, 38054 Grenoble Cedex, France

Received July 28, 1999

Abstract: A correlation between the magnetic properties and the crystal structure of the nitronyl nitroxide (NN) radical 2-(6-ethynyl-2-pyridyl)-4,4,5,5-tetramethylimidazoline-1-oxyl-3-oxide (6-HC≡CPyNN, **1**) and its imino nitroxide analogue 2-(6-ethynyl-2-pyridyl)-4,4,5,5-tetramethylimidazoline-1-oxyl (6-HC≡CPyIN, **2**) has been shown. Magnetic susceptibility measurements on these compounds are indicative of ferromagnetic interactions between molecular units. The imino nitroxide **2** is an organic ferromagnet with critical temperature $T_C = 0.19$ K, whereas **1** behaves as an antiferromagnet ordering at the Néel temperature, $T_N = 0.54$ K. Compounds **1** and **2** are isostructural and crystallize in the $P2_1/n$ space group. Their crystal packings are best described as chains of molecules linked by C≡CH···O hydrogen bonds running along the $[\bar{1}01]$ direction. A comparative analysis of the structures and magnetic properties of both compounds suggests that the coupling between the molecular units along the chain is ferromagnetic. Thus, the magnetic susceptibilities of **1** and **2** have been interpreted in terms of isotropic ferromagnetic Heisenberg linear chains of $S = 1/2$ spins. Weak values of the coupling constants ($J = +0.90$ K for **1**, $J = +0.67$ K for **2**) have been obtained. The spin density distribution of radical **1** has been determined by a polarized neutron diffraction experiment to gain more insight into the mechanism of transmission of magnetic interactions. As in other NN radicals, the spin density is concentrated in the two nitroxide groups and a small negative population is observed in the central carbon atom of the O−N−C−N−O fragment. However, two striking differences with respect to other nitroxides so far studied have been detected. First, the spin density is not equally shared between the two N−O functions. The oxygen atom O1, which participates in the formation of the hydrogen bond, is less populated than the "free" oxygen, O2. Ab initio spin density calculations clearly show that this effect is correlated to the presence of C≡CH···O hydrogen bonds in the crystal. Second, a positive spin density has been detected in the ethynylic hydrogen atom, H16. These two features indicate a spin density transfer from one nitroxide group to the alkyne function of the neighboring molecule.

Introduction

Molecular magnetism is a rapidly developing field that combines the skills of experimental and theoretical scientists in many areas of chemistry.[1,2] It was in the late 1980's that researchers in this field paid attention for the first time to Ullman et al.'s nitronyl nitroxide (NN) free radicals[3] owing to their bidentate character. Coordination of these weakly basic entities to acidic metal centers (e.g., hexafluoroacetylacetonates) led to the formation of ferro- and ferrimagnetic metal−radical alternating chains that order ferromagnetically at low temperatures.[4,5] The so-called *metal−radical approach* to molecular magnets has been extended to nonacidic metal centers by incorporating the NN moiety into a ligand.[6−10] Complexation to the metal center is then driven by the *chelate effect*.

⊥ Present address: Universitat de València, Departament de Química Inorgànica. Dr. Moliner, 50. E, 46100, Burjassot (València), Spain. E-mail: Fco.Manuel.Romero@uv.es; Institut Laue Langeuin, BP156, 38042 Grenoble Cedex, France. E-mail: pontillo@ill.fr.

† ECPM-Strasbourg.

‡ DRFMC/SPSMS/MDN CEA-Grenoble.

Paul Scherer Institute Zürich.

§ DRFMC/SCIB CEA-Grenoble.

|| CRTBT-CNRS Grenoble.

(1) *Molecular Magnetism: From Molecular Assemblies to the Devices*; Coronado, E., Delhaès, P., Gatteschi, D., Miller, J. S., Eds.; NATO Advanced Study Institute Series E321; Kluwer Academic Publishers: Dordrecht, The Netherlands, 1996.

(2) Kahn, O. *Molecular Magnetism*; VCH: New York, 1993.

(3) Ullman, E. F.; Osiecki, J. H.; Boocock, D. G. B.; Darcy, R. *J. Am. Chem. Soc.* **1972**, *94*, 7049.

(4) Caneschi, A.; Gatteschi, D.; Sessoli, R.; Rey, P. *Acc. Chem. Res.* **1989**, *22*, 392.

(5) Caneschi, A.; Gatteschi, D.; Rey, P. *Prog. Inorg. Chem.* **1991**, *39*, 331.

10.1021/ja992673r CCC: $19.00
Published on Web 02/03/2000

Chart 1

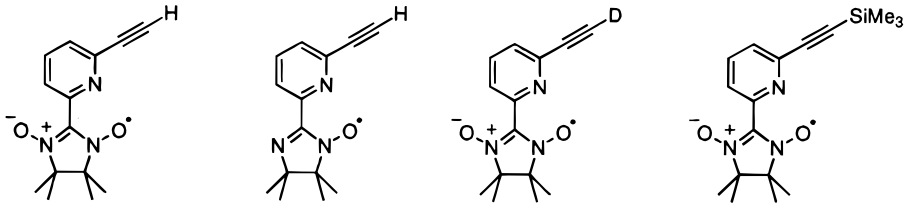

1 **2** **3** **4**

NN radicals regained new interest after the discovery of ferromagnetism at a critical temperature $T_C = 0.6$ K in the β-phase of the (*p*-nitrophenyl) derivative (β-*p*NPNN).[11] Since then, ferromagnetic order has been observed in other nitroxide compounds,[12−17] the highest critical temperature known to date corresponding to a diazaadamantane dinitroxide[18] ($T_C = 1.48$ K). Magnetic ordering in these compounds is driven by the existence of intermolecular interactions. The mechanisms providing their basis are a subject of controversy. Two proposals introduced by McConnell are being generally invoked to ascribe magnetic interactions to a particular intermolecular contact.[19,20] The first one (McConnell's I mechanism) is based on the *spin-polarization effect* and establishes that ferromagnetic (antiferromagnetic) coupling is mediated by the presence of intermolecular contacts between atoms carrying spin densities of opposite (equal) sign. The second one (McConnell's II mechanism) involves mixing with intermolecular charge-transfer excited states. Within this frame, antiferromagnetic coupling is explained in terms of SOMO−SOMO contacts between neighboring molecules, whereas SOMO−lowest unoccupied molecular orbital (LUMO) or SOMO−next highest doubly occupied molecular orbital (NHOMO) contacts induce ferromagnetic interactions. An alternative and elegant view of magnetic exchange in these systems relies on simple molecular orbital (MO) considerations.[21]

MO theoretical studies also revealed that the propagation of magnetic coupling from one molecule to another strongly depends on their mutual orientation and distance.[22] The main challenge for chemists is then to assemble the spin carriers in a crystal lattice in such a way that ferromagnetic interactions are effective. Recently, much progress has been made in the development of synthetic methods for the rational design of molecular crystals.[23,24] These methods (referred as *crystal engineering tools*) rely on the presence of hydrogen bonds, π-π stacking, or strong dipolar interactions. Examples of purely organic ferromagnets engineered by means of hydrogen bonding are known in the literature.[14] It seems that hydrogen bonds play a major role in the propagation of magnetic interactions in these systems.[25] Terminal alkyne functions are also known to favor hydrogen bonding in crystals[26,27] and we may anticipate that C≡CH···O bonds will offer a particularly effective pathway for conduction of magnetic interactions.

However, the prediction of the whole crystal packing from the molecular structure of compounds is not a trivial task.[28] Also, and despite all the efforts devoted to the synthesis and the study of the solid-state properties of NN radicals, it is still not obvious to ascribe their magnetic behavior to a particular structural pattern. In this context, it is necessary to keep in mind the recent report from Novoa and co-workers, who clearly showed that it is not possible to correlate the magnetic properties of a NN radical to the relative spatial arrangement of nitroxide moieties belonging to neighboring molecules.[29]

It is clear that further work aimed at the correlation between structure and magnetism should be done. We think that the systematic search and study of structurally similar compounds showing disparate magnetic behavior may be a rational approach for this purpose. In fact, magnetostructural correlations in inorganic systems began in this way. In preliminary communications[16,30] we have explained the magnetic behaviors of compounds 2-(6-ethynyl-2-pyridyl)-4,4,5,5-tetramethylimidazoline-1-oxyl-3-oxide (6-HC≡CPyNN, **1**) and 2-(6-ethynyl-2-pyridyl)-4,4,5,5-tetramethylimidazoline-1-oxyl (6-HC≡CPyIN, **2**) on the basis of ferromagnetic chains built by weak C≡CH···O bonds. We report now a comparative analysis of both radicals showing that these hydrogen bonds are of the utmost importance for the transmission of ferromagnetic interactions in these systems. Strong evidence for this is supported by a full magnetostructural correlation including magnetic measurements at very low temperatures, polarized neutron diffraction studies, and ab initio spin density calculations.

(6) Luneau, D.; Risoan, G.; Rey, P.; Grand, A.; Caneschi, A.; Gatteschi, D.; Laugier, J. *Inorg. Chem.* **1993**, *32*, 5616.
(7) Luneau, D.; Romero, F. M.; Ziessel, R. *Inorg. Chem.* **1998**, *37*, 5078−5087.
(8) Fegy, K.; Luneau, D.; Ohm, T.; Paulsen, C.; Rey, P. *Angew. Chem., Int. Ed. Engl.* **1998**, *37*, 1270.
(9) Fegy, K.; Sanz, N.; Luneau, D.; Belorizky, E.; Rey, P. *Inorg. Chem.* **1998**, *37*, 4518−4523.
(10) Fegy, K.; Luneau, D.; Belorizky, E.; Novak, M.; Tholence, J.-L.; Paulsen, C.; Ohm, T.; Rey, P. *Inorg. Chem.* **1998**, *37*, 4524.
(11) Kinoshita, M.; Turek, P.; Tamura, M.; Nozawa, K.; Shiomi, D.; Nakazawa, Y.; Ishikawa, M.; Takahashi, M.; Awaga, K.; Inabe, T.; Maruyama, Y. *Chem. Lett.* **1991**, 1225.
(12) Sugawara, T.; Matsushita, M. M.; Izuoka, A.; Wada, N.; Takeda, N.; Ishikawa, M. *J. Chem. Soc., Chem. Commun.* **1994**, 1723.
(13) Nogami, T.; Ishida, T.; Tsuboi, H.; Yoshikawa, H.; Yamamoto, H.; Yasui, M.; Iwasaki, F.; Iwamura, H.; Takeda, N.; Ishikawa, M. *Chem. Lett.* **1995**, 635.
(14) Cirujeda, J.; Mas, M.; Molins, E.; Lanfranc de Panthou, F.; Laugier, J.; Park, G. P.; Paulsen, C.; Rey, P.; Rovira, C.; Veciana, J. *J. Chem. Soc., Chem. Commun.* **1995**, 709.
(15) Caneschi, A.; Ferraro, F.; Gatteschi, D.; Le Lirzin, A.; Novak, M. A.; Rentschler, E.; Sessoli, R. *Adv. Mater.* **1995**, *7*, 476.
(16) Romero, F. M.; Ziessel, R.; Drillon, M.; Tholence, J.-L.; Paulsen, C.; Kyritsakas, N.; Fischer, J. *Adv. Mater.* **1996**, *8*, 826.
(17) Togashi, K.; Imachi, R.; Tomioka, K.; Tsuboi, H.; Ishida, T.; Nogami, T.; Takeda, N.; Ishikawa, M. *Bull. Chem. Soc. Jpn.* **1996**, *69*, 2821.
(18) Chiarelli, R.; Novak, M. A.; Rassat, A.; Tholence, J.-L. *Nature* **1993**, *363*, 147−149.
(19) McConnell, H. M. *J. Chem. Phys.* **1963**, *39*, 1910.
(20) Kollmar, C.; Kahn, O. *Acc. Chem. Res.* **1993**, *26*, 259.
(21) Yoshizawa, K.; Hoffmann, R. *J. Am. Chem. Soc.* **1995**, *117*, 6921.
(22) Yamaguchi, K.; Okumura, M.; Maki, J.; Noro, T.; Namimoto, H.; Nakano, M.; Fueno, T.; Nakasuji, K. *Chem. Phys. Lett.* **1992**, *190*, 353.
(23) Desiraju, G. R. *Angew. Chem., Int. Ed. Engl.* **1995**, *34*, 2311.
(24) Desiraju, G. R. *Chem. Commun.* **1997**, 1475.
(25) Cirujeda, J.; Hernández-Gasió, E.; Rovira, C.; Stanger, J.-L.; Turek, P.; Veciana, J. *J. Mater. Chem.* **1995**, *5*, 243.
(26) Galoppini, E.; Gilardi, R. *Chem. Commun.* **1999**, 173.
(27) Robinson, J. M. A.; Phip, D.; Kariuki, B. M.; Harris, K. D. M. *Chem. Commun*. **1999**, 329.
(28) Gavezzotti, A. *Acc. Chem. Res.* **1994**, *27*, 309.
(29) Deumal, M.; Cirujeda, J.; Veciana, J.; Novoa, J. J. *Adv. Mater.* **1998**, *10*, 1461.
(30) Romero, F. M.; Ziessel, R.; De Cian, A.; Fischer, J.; Turek, P. *New J. Chem.* **1996**, *20*, 919.

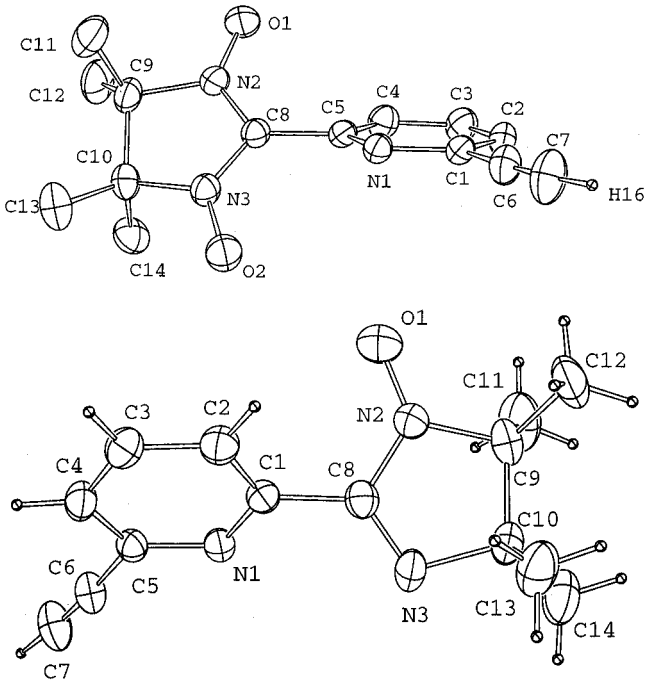

Figure 1. ORTEP views of compound **1** (a) and **2** (b), showing the numbering of the atoms.

Experimental Section

Materials. Compounds **1** and **2** were synthesized from commercially available 2,6-dibromopyridine as previously described.[16,30] **3** was prepared by treatment of 2-(6-trimethylsilylethynyl-2-pyridyl)-4,4,5,5-tetramethylimidazolidine-1-oxyl-3-oxide (**4**) with potassium fluoride in MeOD. The characterization of **3** revealed the presence of a small amount of undeuterated material. EI-MS (Da/e): 258 (21%), 259 (100%), 260 (19%), IR (cm^{-1}): 3228.0 (CC−H), 2552.1 (CC−D), 1958.3 (C≡CD).

Methods. IR spectra of $CDCl_3$ solutions of compounds **1**−**4** were recorded in a IFS-25 Bruker spectrometer using KBr cells. Solid samples were measured on KBr pellets.

Magnetic Measurements. The low-temperature magnetic properties were measured using a low-temperature−high field SQUID magnetometer developed at the CRTBT-CNRS in Grenoble. The magnetometer is equipped with an 8T superconducting magnet and a Nb−Ti shield for field stabilization. Samples are attached to a copper coil foil sample holder, which in turn is thermally anchored to the bottom of a miniature dilution refrigerator that can operate at temperatures down to 0.05 K. The samples can be extracted through the superconducting gradiometer of the SQUID, thus giving absolute values of the magnetization at very low temperature. At low field values the magnetic field was measured directly with a calibrated hall probe to eliminate the small apparent hysteresis due to the superconducting coil. This is especially important for compound **2**, which undergoes a ferromagnetic phase transition (see below).

Polarized Neutron Diffraction. The experiment was performed on the DN2 polarized neutron diffractometer at SILOE reactor (Grenoble, France). The neutron's wavelength was 1.205 Å. A crystal with dimensions 5 × 1.7 × 1.5 mm^3 was selected. In a first step, it was mounted with the $\vec{a}^*$ axis parallel to the applied H = 8T magnetic field of a cryomagnet. In a second step, the crystal was mounted with the $[0\bar{1}1]$ direction parallel to the field. During all the measurements the sample was maintained at a temperature $T = 4.75$ K. Altogether 196 independent flipping ratios were collected up to $\sin\theta/\lambda = 0.55$ $Å^{-1}$.

Results

Crystal Structures. The room-temperature crystalline structures of compounds **1** and **2** are known from X-ray analysis.[30] The two radicals are isostructural and crystallize in the $P2_1/n$ space group. Figure 1 shows their Oak Ridge thermal ellipsoid plot (ORTEP) views together with the atom numbering.

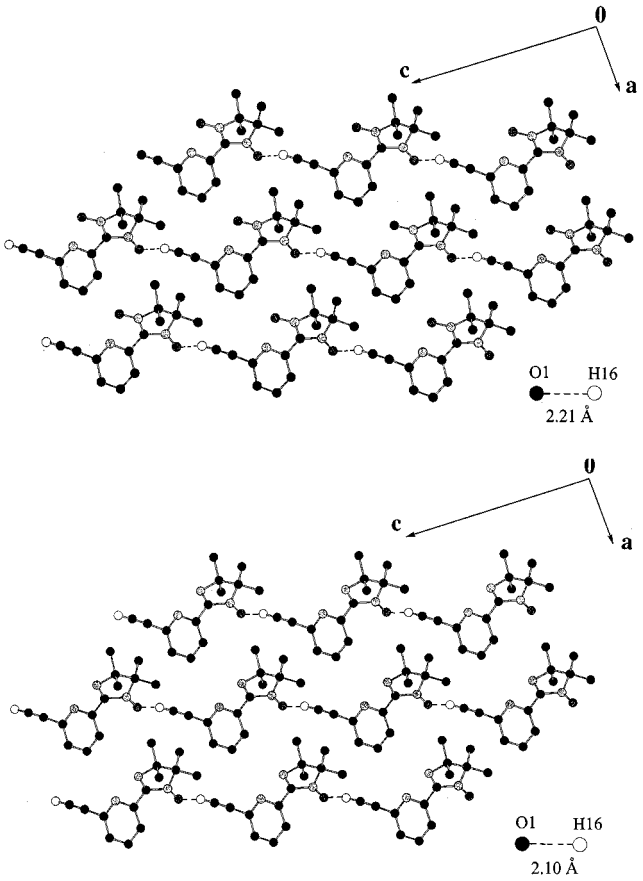

Figure 2. Projection of the crystal structures of compounds **1** (a) and **2** (b) onto the *ac* plane.

6-HC≡CPyNN (1). A projection of the room-temperature crystal structure onto the *ac* plane is shown in Figure 2a. The shortest contact between adjacent molecules [H16···O1 ($x - 1/2$, $1/2 - y$, $1/2 + z$): 2.21 Å] corresponds to a weak C≡C−H···O hydrogen bond so that the packing is best viewed as chains of radicals running along the $[\bar{1}01]$ direction. These chains are linked by short connections between proximate molecules along the *a* axis [N1···H2 ($-1 + x$, y, z): 2.70 Å]. A perpendicular view to the hydrogen-bonded system is shown in Figure 3a together with the unit cell. It shows the spatial arrangement of the chains in a zigzag fashion. Short interchain distances involving the other nitroxyl oxygen O2 and a proton located in the pyridine ring [H1···O2 ($1 - x$, $-y$, $2 - z$): 2.44 Å] are now evidenced. The shortest O···O distance [O1···O2 ($1/2 - x$, $1/2 + y$, $3/2 - z$)] is 4.32 Å. The two N−O bond distances are not equivalent: that corresponding to the N−O function involved in the formation of the hydrogen-bonded chains is larger [N2−O1: 1.284 Å] than the other [N3−O2: 1.269 Å]. The angle between the conjugated plane containing the unpaired electron [O1−N2−C8−N3−O2] and the pyridine mean plane is 47.6°. The dihedral angle between the O−N−C−N−O planes belonging to proximate radicals is 97.6°.

The analysis of unpolarized neutron diffraction at low temperature shows the same crystal symmetry and similar values of the cell parameters.[31] The plane of the pyridine fragment is twisted with respect to the O−N−C−N−O plane by an angle of 45.5° around the C8−C5 bond. The hydrogen-bond length [H16···O1 ($x - 1/2$, $1/2 - y$, $1/2 + z$)] is 2.14 Å.

6-HC≡CPyIN (2). Compounds **1** and **2** are isostructural. Figure 2b shows a projection of the crystal structure of **2** onto

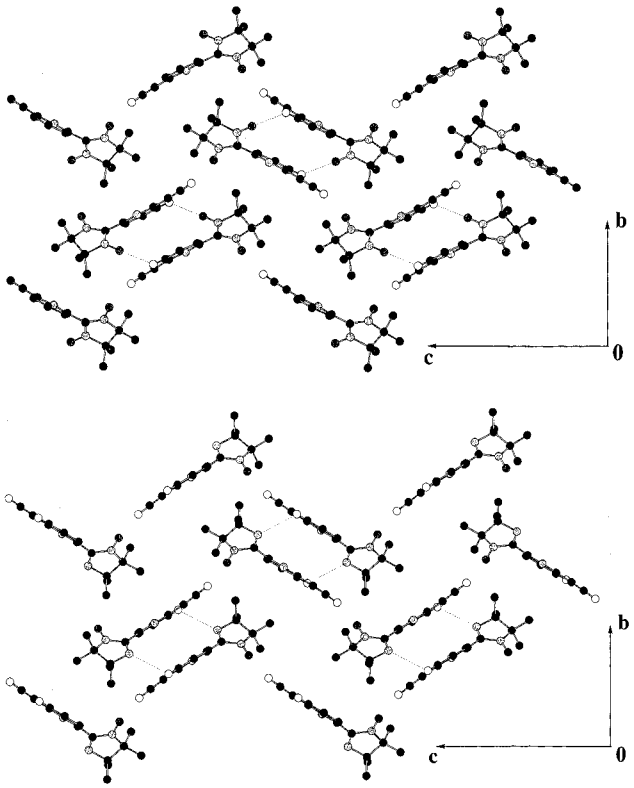

Figure 3. Projection of the crystal structures of compounds **1** (a) and **2** (b) onto the *bc* plane.

the *ac* plane. No remarkable differences with respect to **1** are observed in this view. The hydrogen bond [H16···O1 (*x* − *1/2*, *1/2* − *y*, *1/2* + *z*): 2.10 Å] and the interchain distances along the *a* axis [N1···H2 (−*1* + *x*, *y*, *z*): 2.65 Å] are slightly shorter. A view perpendicular to the *bc* plane (Figure 3b) reveals that the shortest interchain contact involving the radical imine function is larger [N3···H3 (*2* − *x*, −*y*, *1* − *z*): 3.03 Å] than the shortest interchain distance for **1**. At least from a structural point of view, compound **2** has a more pronounced low-dimensional character. The dihedral angle between the [O1−N2−C8−N3] and the pyridine mean planes is 48.5°. The dihedral angle between the O−N−C−N planes belonging to proximate radicals is 87.0°.

Magnetic Properties. 6-HC≡CPyNN (1). Preliminary magnetic measurements were performed between 1.8 and 300 K. At room temperature the product of molar magnetic susceptibility with temperature (χT) equals 0.370 emu·K·mol^{-1}, close to the calculated value for uncorrelated $S = 1/2$ spins. In the whole temperature range the χT product increases smoothly with decreasing temperature, indicating the presence of ferromagnetic interactions. In fact, the field dependence of the magnetization (M) at 1.8 K deviates upward from the Brillouin function for $S = 1/2$. The magnetization curve is best fitted with an effective spin $S_{\text{eff}} = 2$, indicating a spin−spin correlation length of four molecules along the chain at this temperature.

In the very low temperatures region (Figure 4) χT increases also with decreasing temperature until a sharp maximum is reached at 0.61 K, where $\chi T = 1.014$ emu·K·mol^{-1}. Then, χT decreases steadily as T tends to zero. The reciprocal susceptibility ($1/\chi$) (inset, Figure 4) follows a Curie−Weiss law ($\theta = +0.49$ K) in the 8−0.9 K temperature range. Below this temperature $1/\chi$ is nonlinear and shows a critical point at $T_N = 0.54$ K. This behavior is characteristic of dominant ferromagnetic coupling between adjacent molecules to which a very weak antiferromagnetic term is superimposed. Indeed, the thermal variation of χT in the paramagnetic region fits correctly an isotropic one-dimensional ferromagnetic model[32] with $J = +0.90$ K. The maximum is then attributed to antiferromagnetic ordering. This is confirmed by the evolution of M/H as a function of T (Figure 5) for a single crystal in a small applied field of 95 Oe. The sample was first measured along the *a*-axis, which corresponds to the long axis of the needle-shaped crystal. Keeping the same field, the sample was rotated by 90° and remeasured. The peak in M/H corresponds to an antiferromagnetic phase transition at the Néel temperature $T_N = 0.54$ K, and with the easy axis along the crystal *a*-axis direction. This is further supported (Figure 6) by the M versus H measurements performed at $T = 0.075$ K, well below the transition temperature. With H parallel to the *a*-axis, a rather sharp spin-flop type metamagnetic transition can be seen at a critical field of 150 Oe.

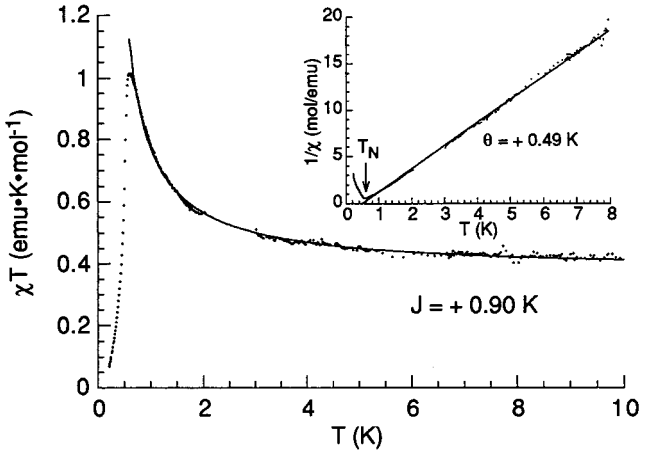

Figure 4. Temperature dependence of the product of the molar magnetic susceptibility with temperature for **1**. *Inset*: Temperature dependence of the reciprocal susceptibility. The solid lines represent the best-fit calculated values.

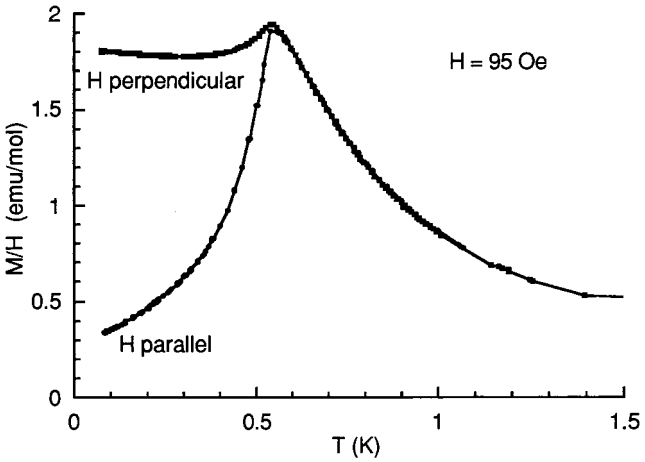

Figure 5. Two M/H versus T curves for a single crystal of compound **1** with the *a*-axis oriented parallel and perpendicular to the magnetic field $H = 95$ Oe.

(31) Crystal data (unpolarized neutron diffraction, $T = 6.5$ K) for **1**: *a* (Å) = 6.283(15); *b* (Å) = 11.811(30); *c* (Å) = 17.526(43); β (deg) = 93.72(11). Atomic coordinates and anisotropic thermal parameters have been refined, from room-temperature values, using the ORXFLS program (see: Busing, W. R.; Martin, K. G.; Levy, H. A. Report O. R. N. L. 59−37; Oak Ridge National Laboratory: Oak Ridge, TN, 1991). The resulting conventional weighting R factor is 0.0604 for 3847 observed reflections (1645 independent) and 316 parameters.

(32) Baker, G. A.; Rushbrooke, G. S.; Gilbert, H. E. *Phys. Rev. A.* **1964**, *135*, 1272.

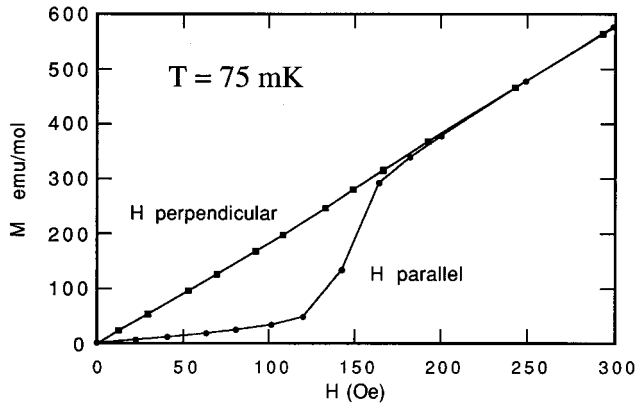

Figure 6. Magnetization curves for compound **1** measured parallel and perpendicular to the easy axis. At approximately 150 Oe there is a spin-flop transition.

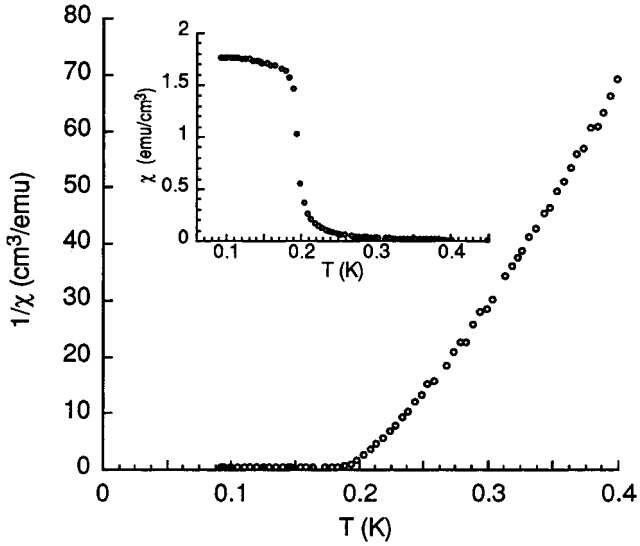

Figure 7. Temperature dependence of the reciprocal susceptibility for **2**. Inset shows the saturation of the applied susceptibility measured in an ac field of 0.7 Oe and at a frequency of 2 Hz.

6-HC≡CPyIN (2). As for **1**, preliminary magnetic measurements in the 1.8−300 K temperature range revealed a global ferromagnetic behavior. Again, the *M* versus *H* curve measured at 1.8 K deviates upward from the Brillouin curve with $S_{eff} = 3/2$.

Susceptibility measurements were made at very low temperatures on a 110 μg single crystal using a small alternating current (ac) field of 0.7 Oe at a frequency of 2 Hz. A small direct current (dc) field was also applied to compensate for the earth's field. The inverse of the applied susceptibility $1/\chi$ decreases continuously upon cooling (Figure 7) and shows a divergence at ca. 0.19 K. The insert of Figure 7 shows the very large value of the applied susceptibility χ_a in emu/cm^3 indicating a ferromagnetic phase transition (for comparison with the previous figures, the applied susceptibility obtains a value of approximately 370 emu/mol at 0.189 K compared to 1.9 emu/mol for compound **1** at the peak). This can been seen in the figure as the saturation of the applied susceptibility to 1/N (the demagnetization coefficient *N* for this long needle-shaped sample is 0.54 ± 0.03, where $\sum N_i = 4\pi$ in cgs units). The thermal variation of χT in the 0.01−5 K temperature range (Figure 8) has been fitted to a ferromagnetic isotropic linear chain of $S = 1/2$ spins with $J = +0.67$ K. A very weak interchain interaction (based on the mean-field approximation[33]) related to $zj' = +0.054$ K slightly improves the fit to data. A good agreement between model and experience is obtained above 0.4 K. Below this temperature χT is field-dependent owing to the proximity of the ferromagnetic region.

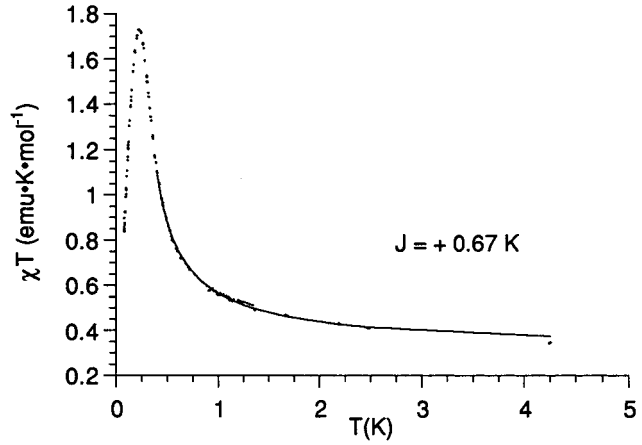

Figure 8. Temperature dependence of the product of the molar magnetic susceptibility with temperature for **2**. The solid line represents the best-fit calculated values.

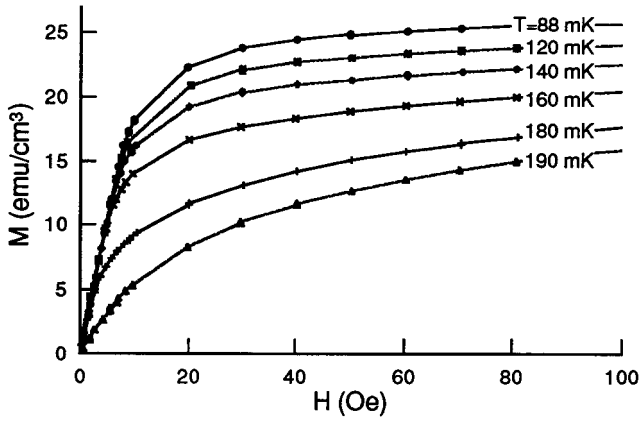

Figure 9. Magnetization curves at the various indicated temperatures for a crystal of compound **2**, measured along the long axis (*a*-axis). Similar curves were obtained along the *b*-axis.

Plots of *M* versus the applied field *H* are shown in Figure 9 for temperatures near T_C. Hysteresis measurements were also made, but no coercive field or remanant moment could be detected within the errors of the magnetometer ($Hc < 1$ Oe). The initial slope of *M* versus *H* for $T < T_C$ saturates to 1/*N*. The spontaneous magnetization is roughly the deviation from this slope at higher field. Scaling plots (see Supporting Information) of the magnetization data give values for the critical exponents $\gamma = 1.28 \pm 0.02$ and $\beta = 0.41 \pm 0.03$ for a $T_C = 0.184$ K ± 0.005. These exponents are reasonable for a ferromagnetic phase transition. However, they are closer to what one would expect for an Ising ferromagnet, as opposed to an isotropic Heisenberg system. A scaling plot of the intrinsic susceptibility (see Supporting Information) has also been performed over a wide range of temperatures in the critical region. Similar values of the critical exponents ($\gamma = 1.27 \pm 0.02$ and $T_C = 0.189$ K ± 0.001) are obtained.

6-DC≡CPyNN (3). It is interesting to compare the magnetic properties of this compound with its nondeuterated analogue (**1**). In the high-temperature limit both compounds exhibit the

(33) Hatfield, W. E.; Weller, R. R.; Hall, J. W. *Inorg. Chem.* **1980**, *19*, 3825.

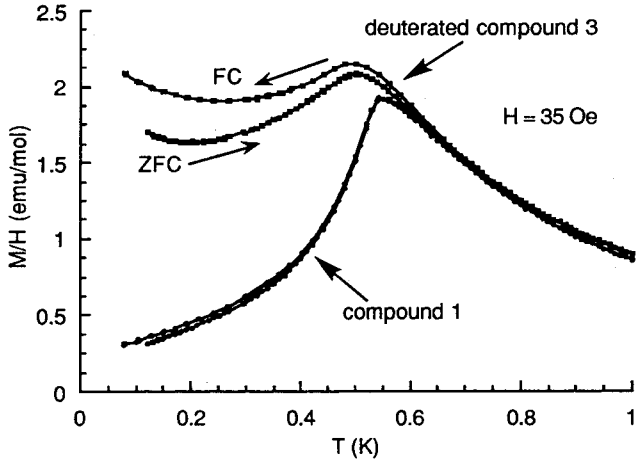

Figure 10. Temperature dependence of *M*/*H* for compound **1** and its deuterated analogue **3**.

same behavior. Below 1 K, however, clear differences are observed. The two *M*/*H* versus *T* curves shown in Figure 10 are for a single crystal of compound **1** measured along the *a*-axis and for a powder sample of the deuterated compound. For these measurements, both samples were placed on the copper sample holder, one above the other about 10 cm apart, and measured at the same time in a field of 35 Oe. To make sure that thermal gradients along the sample holder were negligible the experiment was then repeated, but with the positions of the samples reversed. The results were identical, and an unambiguous difference of approximately 0.05 K is observed between the two peaks. The maximum ($T_N = +0.49$ K) in the *M*/*H* versus *T* curve for **3**, associated with antiferromagnetic ordering, is shifted toward lower temperatures as compared with **1** ($T_N = +0.54$ K). Consequently the zero field cooled (ZFC) susceptibility value at the maximum ($\chi = 2.161$ emu·mol^{-1}) is higher for the deuterated compound. Note also that there is a difference between the ZFC and the field cooled (FC) curves for the deuterated compound. These different behaviors observed below T_N are not well understood.

Above T_N, the χT product for radical **3** fits approximately a one-dimensional isotropic model with an exchange coupling parameter $J = +1.21$ K, to be compared with the value found for **1** ($J = +0.90$ K).

Ab Initio Spin Density Calculations. It is well recognized that the knowledge of the spin density is a crucial point to understand magnetic couplings in materials. This prompted us to calculate theoretical spin density distributions on radicals 6-HC≡CPyNN (**1**) and 6-HC≡CPyIN (**2**). In this section we present the results of ab initio calculations for both compounds, as *isolated molecules*, in the geometry determined experimentally in the crystals (for **1**: unpolarized neutron diffraction at $T = 6.5$ K; for **2**: X-ray diffraction at room temperature).

Two types of ab initio methods are currently used to calculate spin densities of molecular compounds: (a) The Hartree−Fock approaches,[34] and (b) those based on density functional theory (DFT).[35] Zheludev et al.[36] have shown that the results obtained by density functional calculations are more realistic and very stable with respect to the choice of basis and functional. We have then performed calculations with the DFT method as implemented in the program DGAUSS.[37] This program uses Gaussian basis sets. The calculations were done with local spin-density-optimized basis sets at the TZ94+P level.

Table 1. Ab Initio Atomic Spin Populations in **1**

atoms	populations (μ_B)
O1	0.270
N2	0.212
C8	−0.086
N3	0.230
O2	0.312
H16	0.000
C7	0.001
C6	0.001
C1	−0.003
C2	−0.005
C3	0.004
C4	−0.003
C5	0.014
N1	−0.006
C9	0.002
C10	0.008
C11	0.019
C12	0.007
C13	0.007
C14	0.020

Table 2. Ab Initio Atomic Spin Populations Found in O−N−C−N−O Fragments of **A**, **B**, and **1**

atoms	case **A**	case **B**	6-HC≡CPyNN
O1	0.269	0.295	0.270
N2	0.212	0.211	0.212
C8	−0.086	−0.078	−0.086
N3	0.230	0.231	0.230
O2	0.313	0.288	0.312

6-HC≡CPyNN (1). The individual spin populations of H16, O, N, and C atoms are listed in Table 1. The main part of the spin density is carried by the O1−N2−C8−N3−O2 fragment of the nitroxide ring, as previously described for this class of NN compounds.[36] The corresponding central carbon atom, C8, carries a negative spin density (−0.086 μ_B) that corresponds roughly to one-third of the average of the spin populations of the O1, N2, N3, and O2 atoms. In addition, a weak spin delocalization is obtained on the pyridine ring and on the carbon atoms of the acetylenic group: C6, 0.001 μ_B; C7, 0.001 μ_B. No spin density is localized on the H16 hydrogen atom.

The principal feature emerging from these results is the existence of some asymmetry, in terms of spin populations, between O1 (0.270 μ_B) and O2 (0.312 μ_B) oxygen atoms. This asymmetry can be attributed either to the relative position of the ethynyl group or to the position of the nitrogen atom, N1, on the pyridine ring. To elucidate this point, we have performed the same ab initio spin density calculations for two extra (**A** and **B**) model molecules. First, the position of the ethynyl function was changed. In molecule **A** the ethynyl group is now bonded to the C2 carbon atom instead of C1. The spin populations of O1, N2, C8, N3, and O2 atoms are listed in Table 2, together with the corresponding data for **1**. No changes in the spin population values of the O1−N2−C8−N3−O2 fragment are observed. In molecule **B**, the positions of C4 and N1 were permuted versus compound **1**. The calculated spin populations of O1, N2, C8, N3, and O2 atoms are also displayed in

(34) Shawitt, I. Methods of Configuration Interaction. In *Modern Theoretical Chemistry*; Shaefer, H. F., III, Ed.; Plemum Press: New York, 1977; Vol 3, p 189.

(35) Kohn, W.; Sham, L. J. *Phys. Rev.* **1965**, *140*, A1133.

(36) Zheludev, A.; Barone, V.; Bonnet, M.; Delley, B.; Grand, A.; Ressouche, E.; Rey, P.; Subra, R.; Schweizer, J. *J. Am. Chem. Soc.* **1994**, *116*, 2019.

(37) DGAUSS UniChem4, Cray Research Inc., Cray Research Park, 655 Lone Oak Dr., Eogan, MN.

(38) Zheludev, A.; Bonnet, M.; Delley, M.; Grand, A.; Luneau, D.; Örström, L.; Ressouche, E.; Rey, P.; Schweitzer, J. *J. Magn. Magn. Mater.* **1995**, *145*, 293.

Table 3. Ab Initio Atomic Spin Populations in **2**

atoms	populations (μ_B)
O1	0.403
N2	0.315
C8	−0.102
N3	0.277
H16	0.000
C7	0.000
C6	0.000
C1	−0.002
C2	−0.003
C3	0.001
C4	0.009
C5	0.013
N1	−0.004
C9	0.008
C10	0.023
C11	0.034
C12	0.015
C13	0.006
C14	0.015

Table 2. The asymmetry between O1 and O2 spin densities is now reversed as compared to **1**: the spin population on O1 (0.295 μ_B) becomes slightly higher than that calculated for O2 (0.288 μ_B). These calculations at the molecular level show that the spin density is unequally distributed between the two oxygen atoms of compound **1**. It is clear that for the isolated molecule this asymmetry results from the relative position of the nitrogen atom N1 on the pyridine cycle.

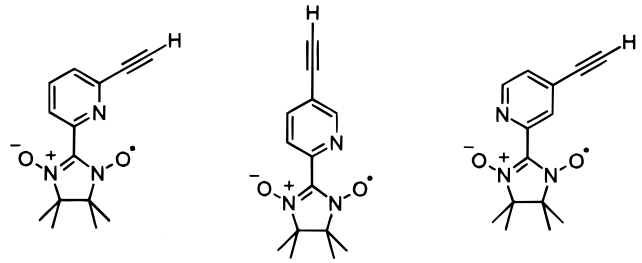

1 **A** **B**

6-HC≡CPyIN (2). The individual spin populations of H16, C, N, and O atoms are listed in Table 3. As already found for this type of compound, most of the spin density is concentrated on the N3−C8−N2−O1 fragment, with a negative density on the bridging sp^2 carbon atom, C8 (−0.102 μ_B). The main observation to be pointed out, when comparing with the NN analogue, is the fact that the spin density is not equally shared between the oxygen and nitrogen atoms of the nitroxide function. It appears to be displaced toward the O1 oxygen atom (N3: 0.277 μ_B; N2: 0.315 μ_B; O1: 0.403 μ_B). Besides this, as in compound **1**, delocalization of the unpaired electron on the pyridine fragment is weak. The spin population calculated for the C6−C7−H16 ethynyl group is exactly zero.

Polarized Neutron Diffraction. We have checked the validity of the above calculations by measuring experimentally the spin density on a single crystal of one of the two species, namely the compound 6-HC≡CPyNN, by polarized neutron diffraction. Such studies on paramagnetic single crystals are possible by inducing a magnetization density by means of a strong vertical magnetic field at low temperature. In practice one measures the so-called *flipping ratios R* of Bragg reflections, that is, for each *hkl* reflection, the ratio of scattered intensities for up (parallel to the applied field) and down (antiparallel) polarizations of the incident beam. If the crystal structure is centrosymmetric, both F_M (magnetic structure factor) and F_N (nuclear structure factor) are real quantities, the expression for R is then given by:

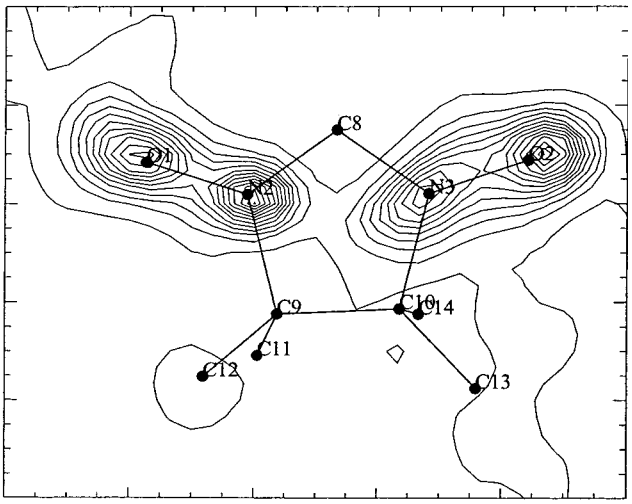

Figure 11. Projection of the MaxEnt reconstructed spin density onto the nitroxide O−N−C−N−O mean plane.

$$R(hkl) = \frac{I^{\uparrow}}{I^{\downarrow}} = \frac{F_N^2 + \sin^2 \alpha\, F_M^2 + 2\sin^2 \alpha\, F_N F_M}{F_N^2 + \sin^2 \alpha\, F_M^2 - 2\sin^2 \alpha\, F_N F_M} \qquad (1)$$

where α is the angle between the scattering vector (*hkl*) and the vertical axis. Then, if the crystal structure is well known, the F_N are known quantities and the magnetic structure factors can be directly extracted from eq 1.

The magnetic structure factors F_M, deduced from the flipping ratios, are the Fourier components of the spin density $S(r)$. There are several methods to reconstruct the distribution $S(r)$. The first one, the maximum entropy method (MEM), is a model-independent approach in the sense that the distribution is reconstructed without any assumption on its nature. It is based on the theory of information and the Bayesian probabilities,[39] and has been previously extended to interpret polarized neutron diffraction data.[40] This technique selects among all the maps consistent with the data the most probable one, that is, the one that maximizes the Boltzmann entropy:

$$\text{entropy}[S(\vec{r})] = -\int_{\text{unit cell}} s(\vec{r}) \ln (s(\vec{r}))d^3\vec{r} \qquad (2)$$

where $s(\vec{r})$ is the spin density normalized to 1 over all the molecule.

In practice one maximizes the functional eq 2 calculated for a three-dimensional spin density map under the constraints $\chi^2 \leq 1$. This method is known to give much better results than the conventional Fourier inversion series, which is the traditional model-independent method of reconstruction.

Figures 11 and 12 show the projection of the MEM reconstructed spin density onto the molecular plane O−N−C−N−O and onto the pyridine ring. As for other NN radicals, most of the density is located on the two nitrogen and the two oxygen atoms of the O−N−C−N−O group. Almost no spin density was detected on the pyridine ring, whereas the acetylenic hydrogen H16 was found to carry a noticeable contribution.

An alternative approach to process the polarized neutron data is to design a parametrized model of the spin density distribution

(39) Skilling, J.; Gull, S. F. In *Maximum Entropy and Bayesian Methods in Inverse Problems*; Smith, R. C., Grandy, W. T., Jr., Eds.; Reidel: Dordrecht, The Netherlands, 1995.

(40) Papoular, R. J.; Gillon, B. *Europhys. Lett.* **1990**, *13*, 429.

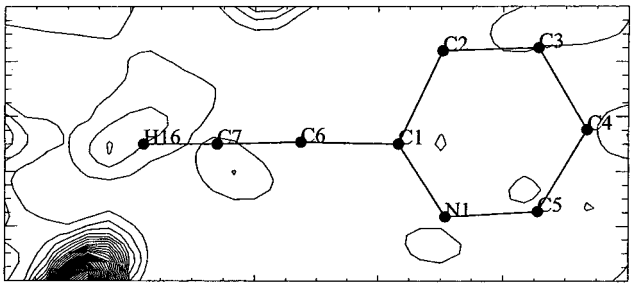

Figure 12. Projection of the MaxEnt reconstructed spin density onto the pyridine ring.

Table 4. Experimental Atomic Spin Populations in **1**[a]

atoms	populations (μ_B)	populations (μ_B)
O1	0.188 (10)	0.203 (10)
N2	0.225 (12)	0.242 (12)
C8	−0.066 (11)	−0.071 (11)
N3	0.209 (11)	0.225 (12)
O2	0.258 (7)	0.278 (7)
H16	0.042 (9)	0.045 (10)
C7	−0.007 (14)	−0.007 (15)
C6	0.028 (13)	0.030 (14)
C1	−0.023 (17)	−0.025 (18)
C2	0.007 (15)	0.007 (16)
C3	0.012 (12)	0.013 (13)
C4	−0.007 (12)	−0.007 (13)
C5	0.002 (15)	0.002 (16)
N1	−0.011 (12)	−0.012 (13)
C9	−0.040 (10)	−0.043 (11)
C10	−0.004 (10)	−0.004 (11)
C11	0.049 (8)	0.053 (9)
C12	0.019 (8)	0.020 (9)
C13	0.019 (9)	0.020 (10)
C14	0.028 (7)	0.030 (7)
sum	0.928 (11)	1.000 (12)
χ^2	1.48	

[a] The second column shows the normalized values.

and to refine the parameters that best fit the experimental magnetic structure factors F_M. This method allows the detection of very small contributions to the spin density. Nevertheless its adequacy relies on the ability of the model to describe the distribution that has to be restored. We have used here a magnetic wave function model.[41] In this framework the spin density $S(\vec{r})$ is modeled as:

$$S(\vec{r}) = \sum_i S_i \Psi_i(\vec{r}) \Psi_i^*(\vec{r}) \qquad (3)$$

where the atomic wave functions $|\Psi_i\rangle$ are constructed from the standard atomic Slater orbitals at each atomic site i, and where the spin populations S_i may be positive or negative, which means that the spin density may be parallel to the applied fields on certain atoms and antiparallel to this field on others. The individual atomic spin populations S_i as well as the radial exponents ζ of the Slater wave functions for each atomic orbital are the parameters of the model that are refined to fit the experimental results.

For the 6-HC≡CPyNN crystal, the refinement of the wave function model gave a good agreement with the data, with an agreement factor $\chi^2 = 1.48$. The resulting spin populations of p orbitals for N, C, and O atoms, and s orbital for H16, are presented in Table 4. The sum of the spin populations over the whole molecule is 0.928(11) μ_B, to be compared with a magnetization of 0.992 μ_B, measured at 1.8 K under an applied field of 8T. The spin populations, normalized to unity for all the molecule, are also displayed in Table 4. Figure 13 shows the contours for the spin density projected onto the O−N−C−

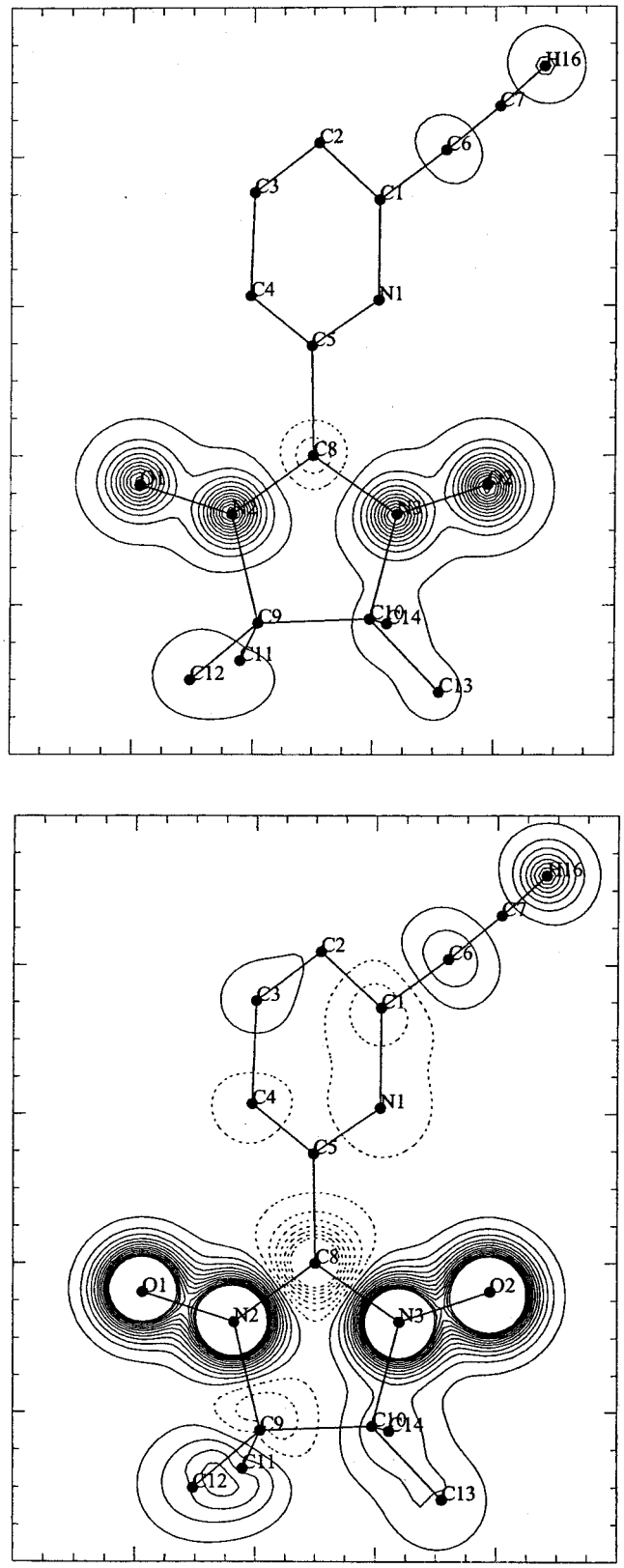

Figure 13. Projection onto the nitroxide O−N−C−N−O mean plane of the high-level (up) and low-level (down) contours of the spin density as analyzed by wave function modeling. Negative contours are dashed.

(41) Gillon, B.; Schweitzer, J. In *Study of Chemical Bonding in Molecules: The Interest of Polarized Neutron Diffraction, Molecules in Physics, Chemistry and Biology*; Maruani, J., Ed.; Kluvwer Academic Publishers: Dordrecht, The Netherlands.

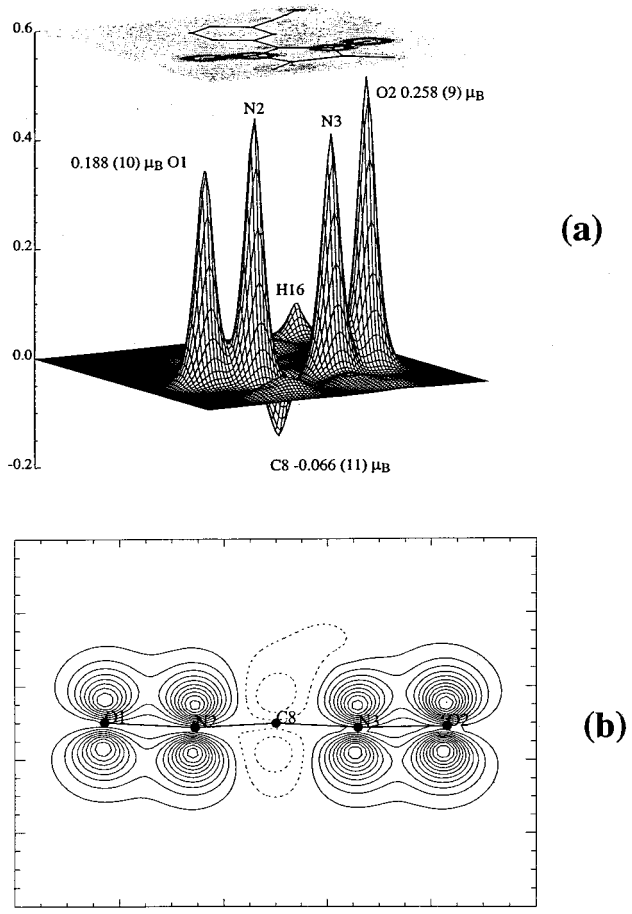

Figure 14. (a) Three-dimensional view of the spin density reconstructed for radical 1 from data obtained by polarized neutrons; (b) projection onto a plane perpendicular to the nitroxide O−N−C−N−O mean plane of the contours of the spin density as analyzed by wave function modeling. Negative contours are dashed.

N−O fragment. A projection onto a plane perpendicular to the O−N−C−N−O plane is represented in Figure 14. The resulting values of the radial exponents ζ are the following: ζ (O) [initial value: 2.25; refined: 2.03 (3)]; ζ (N) [initial value: 1.95; refined: 1.99 (4)]; ζ (C) (not refined: 1.72); ζ (H) (not refined: 1.25).

In accordance with the MEM results, the strongest spin populations are carried by the O−N−C−N−O fragment. As in other NN radicals,[36] but not detected here in the MEM maps, the bridging sp^2 carbon carries a negative spin density ($-0.071\mu_B$) that is in a ($-1/3$) ratio with respect to the average of the spin populations of O1, N2, N3, and O2. The corresponding normalized values for these atoms are, respectively, 0.203, 0.242, 0.225, and 0.278. It is worthy to note that the two oxygen atoms are not equivalent: a transfer occurs from O1 (0.203 μ_B) to O2 (0.278 μ_B). This particular feature of our system is in contrast to the situation found in other NN isolated radicals,[36] but similar to radicals in interaction.[42] Besides this, a significant contribution is found on H16 (0.045 μB), much higher than on the other atoms (except the O−N−C−N−O fragment).

From the Molecule to the Crystal. In the preceding section we have presented the experimental spin density determination of radical **1**. The main features of these results are the asymmetry between O1 and O2 oxygen atoms and the spin density found on the ethynylic hydrogen H16. At this stage, it would be interesting to confirm if these two points are a sign of the active role played by the hydrogen bond O1···H16 in the intrachain coupling. To do that, we have determined the evolution of the ab initio calculated spin density of 6-HC≡CPyNN from the molecule to the crystal via a calculation including two molecules connected through this hydrogen bond.

Table 5. Ab Initio Atomic Spin Populations Found in the O−N−C−N−O Fragment of Radical **1**[a]

atoms	isolated molec.	two molec. connected	crystal	experimental
O1	0.270	0.243	0.239	0.203 (10)
N2	0.212	0.224	0.188	0.242 (12)
C8	−0.086	−0.084	−0.075	−0.071 (11)
N3	0.230	0.230	0.212	0.225 (12)
O2	0.312	0.318	0.312	0.278 (7)
H16	0.000	0.002	0.004	0.045 (10)

[a] Columns refer to calculations made on isolated molecules, on two molecules linked by a hydrogen bond, and on the whole crystal. Experimental values are shown for comparison.

Two Molecules Connected via the Hydrogen Bond H16···O1. These calculations were done using the DFT method (program DGAUSS). The spin populations of O1, N2, C8, N3, O2, and H16 atoms, involved in the hydrogen bond, are presented in Table 5. The experimental values, scaled to 1 μ_B/molecule, and the corresponding spin populations calculated for an isolated molecule are also presented in Table 5 for comparison. Note that the depletion of O1 spin population is emphasized with respect to the isolated molecule. Moreover, a *positive* spin population appears on the hydrogen atom H16. Both the depletion of O1 and the sign of the spin density found on H16 agree with the experimental results. The calculated values, however, are lower than those determined by the experiment.

Crystal. These calculations were performed using the DFT method as implemented in the program DMOL.[43] Table 5 shows the results of DMOL calculations for O1, N2, C8, N3, O2, and H16 atoms of compound **1**, as an isolated molecule and in its crystal environment. The experimental spin populations, scaled to 1 μ_B/molecule, are also shown. As determined above, compared with the isolated molecule, both the depletion of O1 spin population and the positive spin density on the ethynylic hydrogen H16 are obtained. Again, the calculated effects are smaller than those found experimentally.

Discussion

In a first approach, and from a purely phenomenological point of view, a full magnetostructural correlation can be set up by comparing the magnetic properties of the isostructural compounds **1** and **2**. In the paramagnetic region both compounds exhibit ferromagnetic interactions that should be ascribed to the common feature found in their respective crystal packings, that is, the presence of C≡C−H···O hydrogen-bonded chains running along the [$\bar{1}$01] direction. The disparity of behaviors observed at very low temperatures (**1** orders antiferromagnetically at $T_N = 0.54$ K, whereas **2** is a ferromagnet at $T_C = 0.19$ K) is consequently correlated to the difference between these two compounds, namely, the absence of O2 in radical **2**. It is then probable that contacts mediated by O2 could have an impact on the antiferromagnetic ordering observed in the NN compound, although no evidence for this is inferred from the experimental spin density map. Nevertheless it is appropriate to remember that the analysis of the magnetic susceptibility of

(42) Pontillon, Y.; Akita, T.; Grand, A.; Kobayashi, K.; Lelièvre-Berna, E.; Pécaut, J.; Ressouche, E.; Schweizer, J. *J. Am. Chem. Soc.* **1999**, *21*, 10126.

(43) DMOL, Biosym Technologies Inc., 9686 Scranton Rd., San Diego,

both compounds is indicative of very weak interchain coupling, so that the magnetic order in these systems could also be driven by dipolar interactions. An estimate for the dipolar magnetic spin−spin interaction may be obtained from the expression $g^2\mu_B{}^2R^{-3}$, R being the distance between the two interacting radicals. Taking $R = 5.09$ Å, the shortest intermolecular N···O distance, gives an interaction energy of approximately 0.02 K for compound **2**, which is of the same order of magnitude that the interchain coupling derived from the magnetic susceptibility measurements. This approximation gives only an absolute value of the dipolar coupling and precludes any estimation of its sign. Furthermore, dipolar interactions are more diffuse than exchange coupling and this makes it difficult to correlate the long-range order to the microscopic structural features.

An additional proof of the role played by the C≡C−H···O hydrogen bond in the transmission of magnetic interactions is given by the study of the magnetic properties of compound **3**, in which the H atom intervening in the formation of the hydrogen-bonded chains of **1** has been selectively replaced by deuterium. It seems clear, when comparing the ordering temperatures and the J values for **1** and **3**, that the ferromagnetic interaction along the chain is bigger for the deuterated compound. This would mean that the C≡C−D···O bond in **3** is stronger than the C≡C−H···O bond in **1**. This is confirmed by the fact that the shift ($\Delta\bar{\nu}$) observed between the C≡C stretching vibrations of the compounds in the solid state and in dilute solution is bigger for the deuterated compound ($\Delta\bar{\nu} = 30$ cm^{-1}) than for its nondeuterated analogue ($\Delta\bar{\nu} = 15$ cm^{-1}). In some cases, deuterium bonds are stronger than hydrogen bonds. For instance, it has been shown that water dimers in the gas phase have a $H_2O{\cdot}D_2O$ structure, this being around 60 cm^{-1} more stable than the $D_2O{\cdot}H_2O$ form.[44]

Thus, the study of the magnetic properties of compounds **1**−**3** suggests that C≡C−H···O bonds may be responsible for the propagation of ferromagnetic interactions along one-dimensional chains. Further insight into this assumption is given by the measurement of the spin density map for compound **1** and the results of ab initio spin density calculations.

Compared to the spin density found on other NN molecules with no intermolecular magnetic interactions,[36] the spin density measured on radical **1** shows striking differences that may be related to the chain structure of the compound, namely (a) the significant and positive density on the hydrogen atom (H16) involved in the formation of the hydrogen bond and (b) the depletion of density on the oxygen atom O1 of the next molecule to which H16 is bound. We shall now examine carefully, with the help of the different ab initio calculations reported above, whether these particular features are indicative of the ferromagnetic interactions that propagate along the chains.

The normalized spin density found on O1 is 0.203(10), significantly less than the 0.278(7) found on O2. The DFT calculation on the isolated molecule, besides the fact already evidenced[36] that the calculated density is less on the N atoms than on the O atoms of the NN radical, yields 0.270 on O1 and 0.312 on O2 (Table 1). This breaking of symmetry, observed for a single molecule of compound **1** isolated from the chain, is internal and comes either from the relative position of the ethynyl group C≡C−H or from the presence of the nitrogen atom N1 in the pyridine cycle. Table 2 shows that attaching the ethynyl group to C2 instead of C1 practically does not modify the spin densities calculated on O1 and O2. On the opposite, inverting atoms N1 and C4 in the pyridine cycle reverses the balance and the spin density becomes larger on O1 than on O2. We can then consider that the disymmetry of the pyridine cycle is responsible for a lack of balance of 0.03 to 0.04 in favor of O2, that is, half of the difference of 0.075-(12) experimentally observed. It is then natural to think that the second half of this difference is the result of the intermolecular magnetic interactions that propagate along the chain and deplete the O1 spin population. This assertion is confirmed by the examination of Table 5, which compares the spin populations for an isolated 6-HC≡CPyNN molecule with those calculated for several molecules in interaction. Table 5 proposes a difference of 0.027 for a calculation involving two molecules and yields a difference of 0.035 for the interaction when the molecule is inserted in the crystal. These values fit quite well the part of the experimental depletion attributed to the magnetic interactions. Such a spin depletion on an oxygen atom, resulting from magnetic interactions, has already been found in other compounds. This was the case of TEMPOL, where the magnetic interaction was mediated through a hydrogen bond.[45] An even more dramatic example was met in a copper NN complex[46] where a strong interaction with the Cu atom practically canceled the spin density on the bonded nitroxyl oxygen.

Along with the depletion on the O1 oxygen, a positive spin population of 0.045(10) was found on the connected hydrogen (H16). The ab initio calculations (Table 5) show that a spin population appears on H16 when the molecules are in interaction. This spin density clearly results from a delocalization of the density on the oxygen atom due to the magnetic interactions. However, and even if the calculations are able to reproduce the experimental depletion of the spin population in O1, the calculated spin density on H16 is smaller than the experimental value by one order of magnitude. This illustrates the main weakness of the DFT calculations, which are unable to figure out properly the spin density induced by the magnetic interactions on the neighboring molecule.[47]

To summarize, these results strongly support our description of compounds **1** and **2** as hydrogen-bonded chains of radicals. The analysis of the magnetic susceptibility versus temperature curves in terms of a one-dimensional model suggests that the coupling between adjacent molecular units is ferromagnetic. A possible explanation for the sign of this magnetic interaction can be given by considering the SOMO and LUMO orbitals for both molecules (Figure 15). Note that the LUMO is distributed throughout the pyridine ring with a large contribution in the ethynyl fragment. The main role of the H16···O1 hydrogen bond is then to promote an overlap between SOMO and LUMO orbitals belonging to proximate molecules while avoiding intermolecular SOMO−SOMO contacts, as postulated for other hydrogen-bonded open-shell systems.[48] The result is the appearance of a net ferromagnetic interaction, according to McConnell's II mechanism.

Conclusion

Purely organic ferromagnets are structurally isotropic and exhibit very weak interactions. These two facts make the correlations between their structures and their magnetic properties a delicate task. We thought that a rational strategy that would permit us to solve this problem would be the study of the

(44) Engdahl, A.; Nelander, B. *J. Chem. Phys.* **1987**, *86*, 1819.

(45) Bordeaux, D.; Boucherle, J. X.; Delley, B.; Gillon, B.; Ressouche, E.; Schweizer, J. *Z. Naturforsch. A: Phys. Sci.* **1993**, *48a*, 117.

(46) Ressouche, E.; Boucherle, J. X.; Gillon, B.; Rey, P.; Schweizer, J. *J. Am. Chem. Soc.* **1993**, *115*, 3610.

(47) Yamanaka, S.; Kawakami, T.; Nagao, H.; Yamaguchi, K. *Chem. Phys. Lett.* **1994**, *231*, 25.

(48) Hernandez, E.; Mas, M.; Molins, E.; Rovira, C.; Veciana, J. *Angew. Chem., Int. Ed. Engl.* **1993**, *32*, 882.

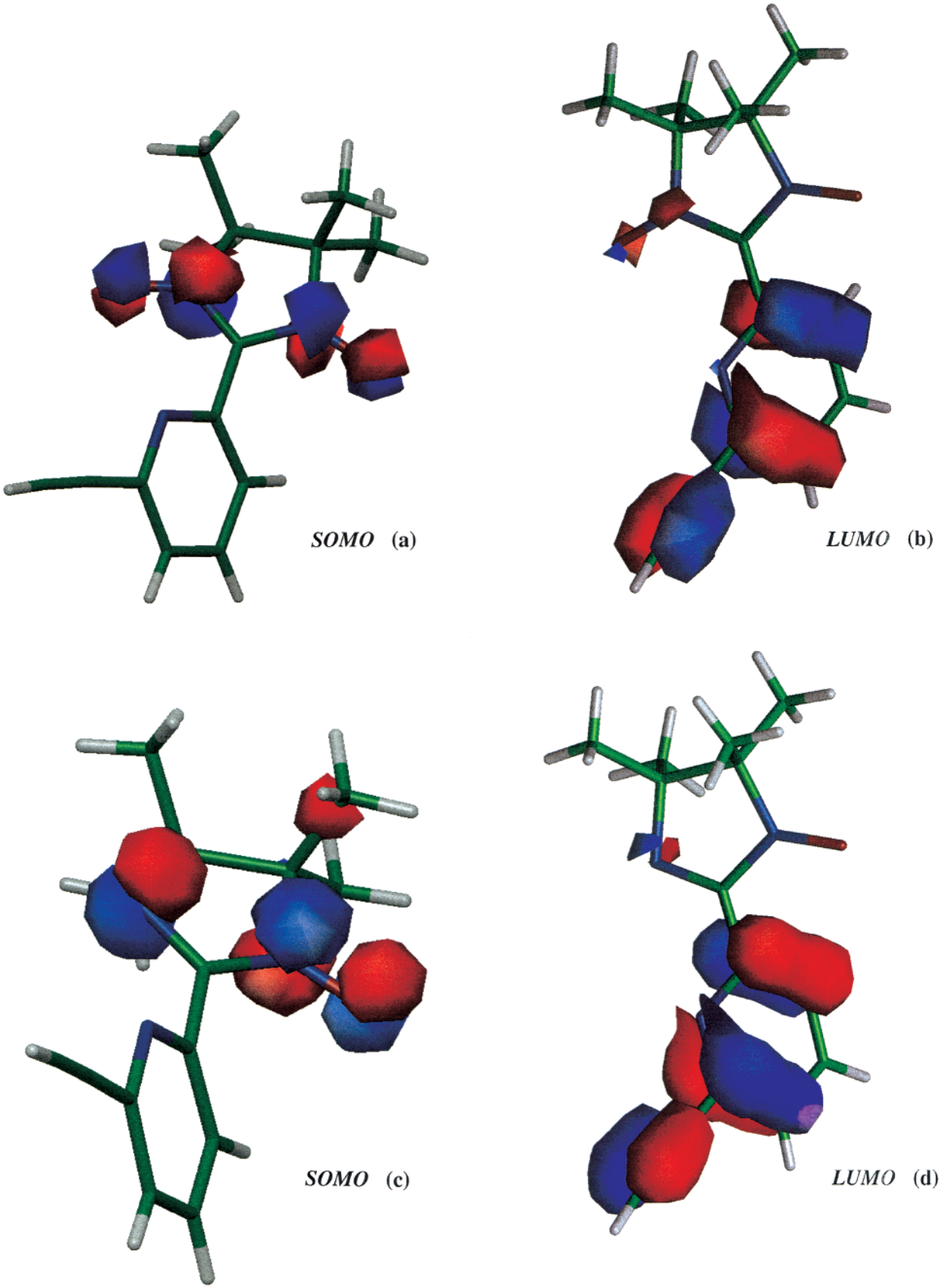

Figure 15. Representation of SOMO and LUMO orbitals for compound **1** (a) and (b) respectively and for compound **2** (c) and (d), respectively.

magnetic properties of very similar isostructural compounds. Our approach is based on a comparison between a NN radical (**1**) and its IN analogue (**2**). Chemically, both compounds only differ by the presence of the O2 oxygen atom in **1**. They are expected to crystallize in the same type of structure, providing that their packing is determined by only one type of hydrogen bond. In the first part of the paper a comparative analysis of the structures and magnetic properties of radicals **1** and **2** has

been presented. It has been shown that the isostructurality between these two compounds is a valuable tool for the determination of the exchange pathways corresponding to the dominant ferromagnetic interactions. The key role played by the hydrogen bonds in the transmission of ferromagnetic interactions along the chains has been confirmed with the study of compound **3**. A clear "isotopic effect" in the susceptibility measurement has been observed.

In this study we have also determined the spin density distribution in a single crystal of compound **1**. As opposed to other cases of NN radicals where the molecules are isolated one from the other, we have seen here the effects of the magnetic interactions that connect neighboring molecules along the chain via the hydrogen bond. The magnetic interaction depletes the spin density on the oxygen atom involved in the formation of the hydrogen bond and delocalizes this spin density on the hydrogen atom of the next molecule in the chain. These effects are confirmed by the ab initio DFT calculations: quantitatively for the depletion on oxygen, but qualitatively only for the delocalization on hydrogen. Such a study shows how polarized neutron diffraction is an important tool in investigating the spin density in magnetic molecular compounds.

Although their existence has been a matter of controversy in the past, it is now recognized that C−H···O hydrogen bonds play a major role in the formation of molecular solids.[49] This contribution provides further evidence into this and shows the importance of C−H···O contacts for the transmission of magnetic interactions.

Acknowledgment. We are pleased to acknowledge Richard Poinsot (IPCMS in Strasbourg) for the preliminary magnetic measurements and Dr. Marc Drillon (IPCMS) for helpful discussions. This work was partially supported by the CNRS and by the Human Capital and Mobility Program of EU (Network: Magnetic Molecular Materials, no. ERBCHRXCT 920080).

Supporting Information Available: Scaling plots in the critical region: critical isotherm ln M versus ln H_i measured at $T = 180$ mK, were H_i is the internal field after corrections for demagnetization effects, and ln χ_i vs ln$(T-T_C)$ plot, χi being the intrinsic susceptibility (PDF). This material is available free of charge via the Internet at http://pubs.acs.org.

JA992673R

(49) Desiraju, G. *Acc. Chem. Res.* **1991**, *24*, 290.